Electrical Transport Properties of $BaWO_4$ under High Pressure

ARTICLE *in* THE JOURNAL OF PHYSICAL CHEMISTRY C · NOVEMBER 2012

Impact Factor: 4.77 · DOI: 10.1021/jp306256k

THE JOURNAL OF PHYSICAL CHEMISTRY C

Article

pubs.acs.org/JPCC

Electrical Transport Properties of $BaWO_4$ under High Pressure

Yuqiang Li,[†] Yang Gao,[†,‡] Yonghao Han,[†] Cailong Liu,[†] Wanbin Ren,[†] Qinglin Wang,[†] Yanzhang Ma,[‡] Baojia Wu,[§] and Chunxiao Gao*[,†]

[†]State Key Laboratory of Superhard Materials, Institute of Atomic and Molecular Physics, Jilin University, Changchun 130012, People's Republic of China

[‡]Department of Mechanical Engineering, Texas Tech University, Lubbock, Texas 79409, United States

[§]College of Science, Yanbian University, Yanji 133002, People's Republic of China

S *Supporting Information*

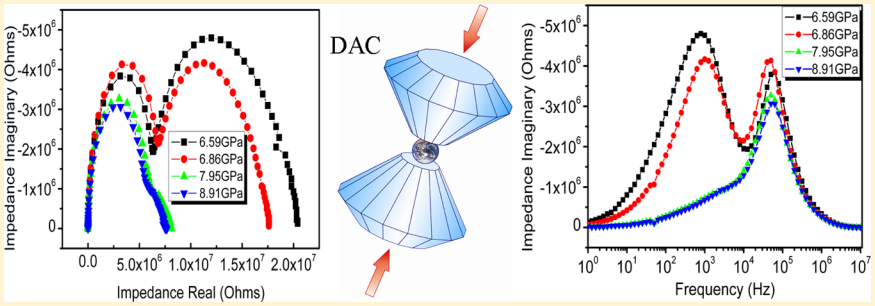

ABSTRACT: An alternate current impedance spectrum was utilized to differentiate the electrical transport process, respectively, in the bulk and the grain boundary of barium tungstate microcrystallines under high pressures up to 20 GPa. For powdered $BaWO_4$ microcrystallines, the grain boundary makes a more remarkable contribution than the bulk to the total resistance. The discontinuities of bulk resistance and relaxation frequency at about 7 and 14 GPa reflect the pressure-induced structural phase transitions of $BaWO_4$ from scheelite to fergusonite structure and from fergusonite to an unknown disordered structure, respectively. The activation energy of the grain boundary decreases with increasing pressure from 6.9 to 8.9 GPa, indicating that the compression has a negative contribution to the activation energy and the transport of charge carriers through the boundary becomes easier. The activation energy of the bulk also shows a similar phenomenon. In addition, the ascending relaxation frequency of the bulk and grain boundary shows that the polarization process needs much shorter time in the state of three-phase coexistence.

1. INTRODUCTION

An alkaline earth tungstate (AWO_4) is an important type of material from both theoretical and technological points of view and has a long history of practical application.[1] Barium tungstate, $BaWO_4$, has attracted a great deal of attention due to its applications in recent years. The $BaWO_4$ crystal is one of the most promising candidates for many technological applications, such as Raman converters and amplifiers.[2,3] In particular, $BaWO_4$ is also known by its unique crystalline property and has been considered for the use of laser with a wide variety of pump pulse durations ranging from nanoseconds to picoseconds.[4] $BaWO_4$ is a wide gap semiconductor with direct band gap energy close to 5.26 eV at ambient condition and is an excellent material for a new generation of cryogenic phonon-scintillation detectors.[5,6] At ambient conditions, $BaWO_4$ has a tetragonal scheelite structure with Ba^{2+} and W^{6+} cations 8-fold and 4-fold coordinated by oxygen, respectively.

Previous investigations revealed many structural phase transitions under high pressure. Jayaraman et al. reported a reversible pressure-induced phase transition in $BaWO_4$ starting at 6.5 ± 0.3 GPa by Raman scattering.[7] Another room-temperature Raman scattering study of $BaWO_4$ allowed Manjón et al. to conclude that the tetragonal scheelite phase ($I41/a$) was transformed into a new monoclinic $BaWO_4$–II phase ($P21/n$) from 6.9 to 9.5 GPa; in the meantime, a further change in the spectrum was observed at 7.5 GPa related to a scheelite-to-fergusonite ($I2/a$) transition, and three phases coexisted within 7.5–9.0 GPa.[6] By in situ angle-dispersive X-ray diffraction experiments, Vinod Panchal et al. showed that $BaWO_4$ existed in the scheelite phase at ambient conditions and transformed to a fergusonite phase rather than $HgMoO_4$ type at 7 ± 0.3 GPa and underwent a second phase transition from the fergusonite phase to a significantly disordered structure above 14 GPa.[8] Errandonea et al. also found that $BaWO_4$ underwent a pressure-driven phase transition at 7.1 GPa from the tetragonal scheelite structure to the monoclinic fergusonite structure by an angle-dispersive X-ray diffraction measurement, and the

Received: June 25, 2012
Revised: October 9, 2012
Published: November 15, 2012

   dx.doi.org/10.1021/jp306256k | *J. Phys. Chem. C* 2012, 116, 25198–25205

Table 1. High-Pressure Results of $BaWO_4$ as Reported in the Literature

	ref 6	ref 8	ref 9
phase	transition pressure (GPa)		
scheelite ($I41/a$)			
$BaWO_4$–II ($P21/n$)	6.9–9.5		
fergusonite ($I2/a$)	7.5	7 ± 0.3	7.1
unknown structure		>14	
pressure-transmitting medium	4:1 methanol–ethanol	4:1 methanol–ethanol or 16:3:1 methanol–ethanol–water	silicone oil
research method	Raman scattering	X-ray diffraction	X-ray diffraction

scheelite structure was predicted to transform under compression directly to a monoclinic structure with space group symmetry $P21/n$ according to their ab initio calculations.[9] Table 1 gives an overview on the pressure-induced phase transition reported in the literature.

As mentioned above, the structural phase transition of $BaWO_4$ under high pressure has been gradually clarified. However, it is also important to understand the electrical transport properties as a wide gap semiconductor. So far, it is still uncertain if structural phase transition of $BaWO_4$ could affect the electrical transport properties under high pressure. High-pressure grain boundary effects and relaxation phenomena still remain unknown and merit further research. In addition, the electrical transport properties of $BaWO_4$ have significant geophysical and geochemical implications in respect to that the initial scheelite-structured orthotungstates are common accessory minerals in various kinds of rocks in the Earth's upper mantle. Especially, the experimental investigation on the electrical transport behavior of $BaWO_4$ under high pressure has not been reported.

In the present study, the electrical transport behaviors of $BaWO_4$ under high pressure have been studied up to about 20 GPa. For getting accurate data, a kind of insulating gasket was developed and employed to avoid introducing additional errors in the experiment. Taking advantage of the highly integrated microcircuits on a diamond anvil cell (DAC), in situ impedance spectrum measurements were conducted, and the bulk and grain boundary effects have been studied. Pressure-induced relaxation frequency and activation energy were also discussed.

2. EXPERIMENTAL SECTION

Commercially available $BaWO_4$ powder with purity of 99.9% was obtained from Sigma-Aldrich Co. The initial phase composition of the sample has been checked by a powder X-ray diffractometer with Cu Kα radiation, and the sample was found to be tetragonal scheelite structure ($I41/a$). Figure 1(a) gives the XRD spectrum of the initial structure, and Figure 1(b) shows that the average size of the crystallites was about 8 μm measured by a scanning electron microscope (SEM).

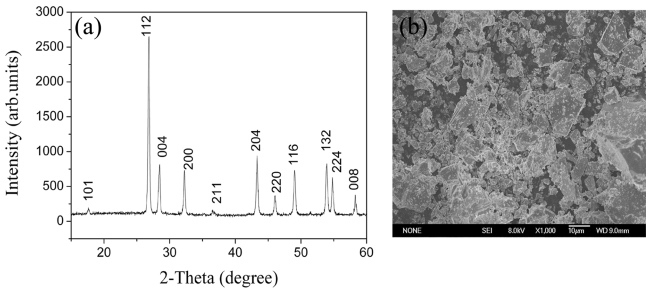

Figure 1. (a) X-ray diffraction pattern of $BaWO_4$ at ambient pressure. (b) The SEM micrograph of the $BaWO_4$ sample.

A DAC was utilized to generate high pressure, and the anvil culet was 300 μm in diameter with a bevel angle of 10°. An integrated thin film microcircuit was used to investigate the impedance spectrum of $BaWO_4$. The manufacturing process of the microcircuit was similar to that reported in our previous work.[10,11] First of all, a molybdenum thin film was deposited on one diamond anvil and then patterned into four detecting electrodes by photolithography technique and chemical etching. The distance between electrodes was 30 μm. An Al_2O_3 layer was deposited on the Mo film by means of the magnetron sputtering technique to protect the Mo electrodes and insulate them from the metal gasket under high pressure. Two diagonally detecting electrodes were used in the experiments, and the result of measurement can be compared with the data by means of another two diagonal electrodes to ensure the correctness of the measurement result.

As for studying electrical properties of materials, the insulating character has a significant effect on results of the experiment. A kind of insulating gasket was used in the experiment to acquire more precise result and eliminate the error brought by the electric short between the sample and inside wall of the gasket. The manufacturing process of the insulating gasket is shown in Figure 2. A preindented T301 stainless steel of 80 μm thickness was used as the gasket floor. Figure 2(a) depicted the indentation of the diamond culet,

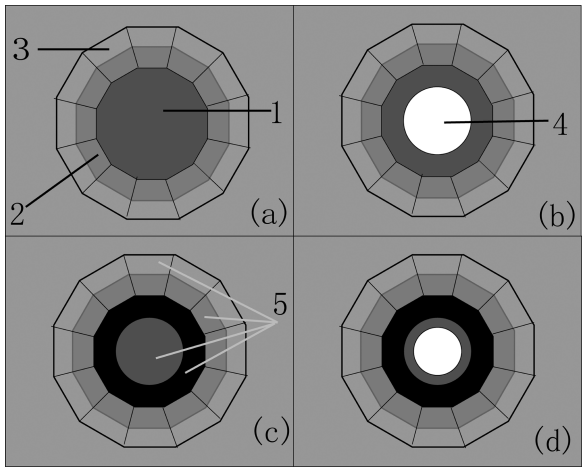

Figure 2. Manufacturing process and the configuration of the insulating gasket. (a) The steel gasket with indentation: (1) indentation of diamond culet, (2) indentation of bevel angle, (3) indentation of side face. (b) Steel gasket with a hole: (4) a hole at the center of the gasket. (c) A lay of diamond powder covers the indentation and fills the hole: (5) diamond powder. (d) The final insulating gasket.

dx.doi.org/10.1021/jp306256k | J. Phys. Chem. C 2012, 116, 25198–25205

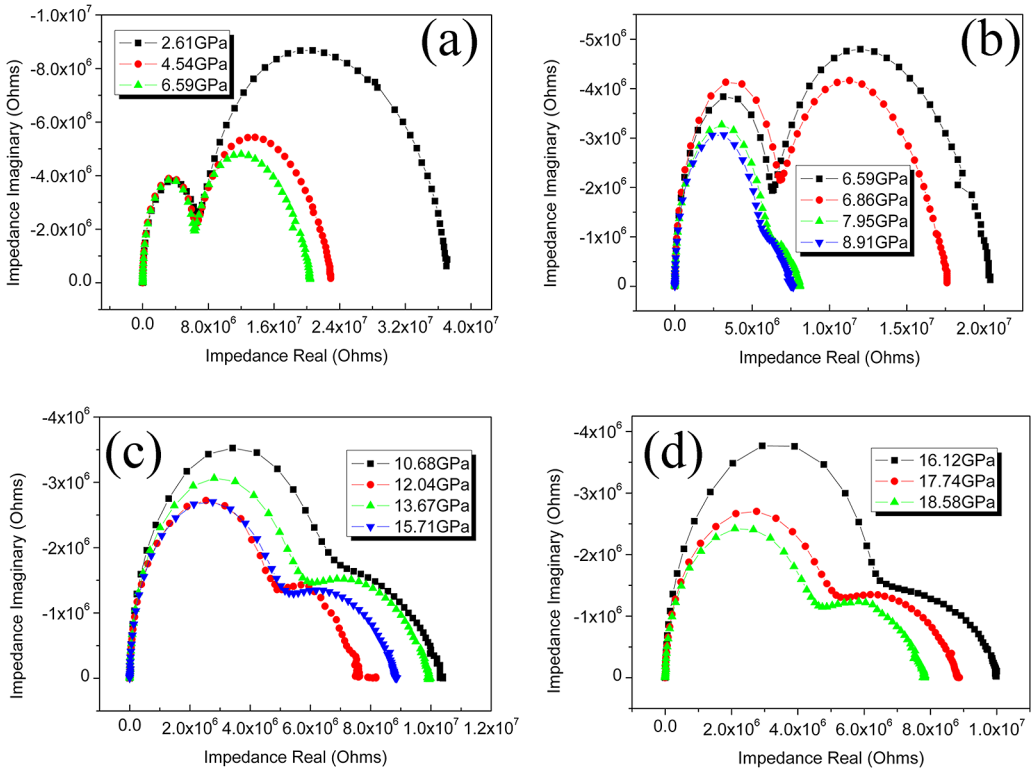

Figure 3. Impedance spectroscopy Z'' vs Z' as a Nyquist diagram for $BaWO_4$ polycrystals at various pressures.

bevel angle, and side face. A hole with 150 μm diameter was drilled at the center of the indentation culet by the action of a laser [Figure 2(b)]. A layer of diamond powder was averagely pressured on the indentation parts of the gasket floor including the diamond culet, bevel angle, and side face; furthermore, the hole was filled completely [Figure 2(c)]. The diamond powder mixed with glue and PMMA (polymethylmethacrylate) was used as the optimal insulating powder. The glue and PMMA can improve the glutinosity and the intensity to enhance the adhesion of the diamond powder layer. Another small hole with 80 μm diameter was drilled at the center of the filled indentation by the same laser beam. The surface and inside wall of the gasket were full of diamond powder, and the insulating effect can be ensured. The final insulating gasket was shown in Figure 2(d). A piece of ruby crystal was placed in the center of the insulating sample chamber as the pressure calibrator.[12] No pressure-transmitting medium was used to avoid introducing additional impedance. The alternate current (ac) impedance spectrum measurements of $BaWO_4$ were carried out by employing the Solartron 1260 impedance spectrometer equipped with the Solartron 1296 dielectric interface with two contact terminals. The frequency ranged from 0.1 to 10^7 Hz. The ac voltage was a 100 mV sine signal for the sake of avoiding the effect of the signal on the inner structure of the sample. To ensure the stability of the sample during the measurement, the indoor temperature was kept constant. The $BaWO_4$ sample was slowly pressurized from ambient pressure to 20 GPa.

3. RESULTS AND DISCUSSION

3.1. Bulk and Grain Boundary Resistances under High Pressure. The complex impedance spectrum is a powerful tool in separating out the bulk and the grain boundary effects. The impedance data collected from $BaWO_4$ polycrystals at various pressures are presented in Figure 3. The real (Z') part and the imaginary (Z'') part of the impedance are obtained from measured amplitude |Z| and phase ϕ determined at a given frequency by $Z' = |Z|\cos\phi$ and $Z'' = |Z|\sin\phi$.

It can be seen in Figure 3(a) that there are partial overlaps between two semicircles. The impedance semicircles become smaller with increasing pressures. Accordingly, the well-defined semicircle at high and low frequencies can be attributed to the charge transport within bulk and at the grain boundary, respectively.[13,14] The observation of two semicircles suggests that the bulk−grain boundary model could be employed for further analysis. The left high frequency arc represents the bulk effect, and the right low frequency arc depicts the grain boundary effect. From the intercept of each semicircular arc with the real axis, the resistance of bulk (R_b) and the resistance of grain boundary (R_{gb}) can be obtained.[15,16] In the pressure range of 2.6−6.6 GPa, the impedance magnitude decreases with increasing pressure, but the shape of the semicircle keeps invariable which implies that the charge transport process smoothly changes with increasing pressure. It should be noticed that the intercepts of the grain boundary arcs obviously decrease in contrast with that of the bulk arcs, indicating that the decrease of impedance magnitude mainly originates from the decline of the grain boundary effect.

When pressure comes up to 6.9 GPa, there are some evident changes in the impedance arcs as shown in Figure 3(b). The total intercepts of impedance arcs start to sharply decrease, and the semicircles of grain boundary arcs change into irregular arcs from well-defined semicircles. The changes indicate the total impedance magnitude decreases, and the decrease mainly comes from the contribution of grain boundary resistance. Furthermore, there is an evident increase in the intercept of the bulk arc that happans at about 6.9 GPa. The decline trend of total impedance magnitude is attributed to the grain boundary

dx.doi.org/10.1021/jp306256k | J. Phys. Chem. C 2012, 116, 25198−25205

effect due to the increase of the bulk arc and decrease of the grain boundary arc. That is to say that the grain boundary effect plays a prominent role in the electrical transport process, and the bulk contribution is subordinate. The total impedance magnitude has an obvious decrease above 6.9 GPa, which reveals the occurrance of structural phase transition. As reported previously, the phase transition of $BaWO_4$ polycrystals from the tetragonal scheelite phase to the fergusonite phase occurred in this pressure range (7 ± 0.3 GPa) by a high-pressure XRD experiment, and it is at about 6.5 ± 0.3 GPa for the Raman scattering study.[8,7] The experimental result indicates the structural transition is first caused by bulk because of an abrupt increase in bulk arc occurring at this pressure and then involves grain boundary. Frequently, the grain boundary effect on the electrical transport process is mainly derived from the grain boundary potential barriers.[17] Pressure-induced phase transition can bring about the rearrangement of atom position and result in the lower systematic energy and more steady lattice structure. The phase transition lowers the grain boundary potential barrier height, and the charge carrier transports more easily through the grain boundary, resulting in the decrease of grain boundary resistance. It is observed that the size of the bulk arc is smaller than that of the grain boundary arc before 6.9 GPa, but this tendency has an obvious reversion above 6.9 GPa. The bulk and grain boundary electrical responses show that the grain boundary resistance plays a primary role in the total $BaWO_4$ impedance from 2.6 to 6.9 GPa.[18]

As shown in Figure 3(c), both the intercepts of bulk arc and grain boundary arc gradually decrease from 7.9 to 13.7 GPa. However, the intercept of the impedance arc has an obvious increase with pressure beyond 13.7 GPa. The abrupt increase can be attributed to the structural phase transition from the fergusonite phase to an unknown disordered phase at about 14 GPa.[8] The whole shape of impedance arc has no evident change in the pressure zone of 7.9−13.7 GPa, indicating the phase transition occurs after 13.7 GPa. From 15.7 to 18.6 GPa, the shape of the impedance arc almost keeps changeless, and the intercept of the impedance with real axis equally decreases with increasing pressure as shown in Figure 3(d).

To get more information relative to electrical transport properties, the ZIEW2 impedance analysis software was used to analyze the experimental data. The pressure-dependent R_b and R_{gb} are shown in Figure 4 in which the resistances data were obtained by the equivalent circuit model with two parallel $R-C$ elements. The high-frequency contribution from the first $R-C$ elements can be identified as the bulk response, and the low-frequency contribution from the second $R-C$ elements corresponds to the grain boundary contribution.

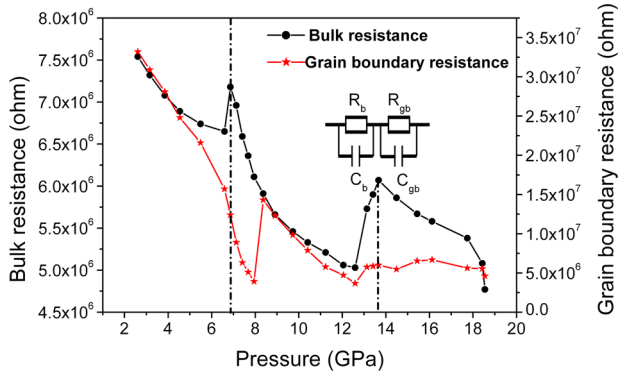

Figure 4. Pressure dependence of the bulk resistance and grain boundary resistance of $BaWO_4$ at room temperature. Inset: An equivalent electrical circuit including resistor R and capacitor C elements composed of two parallel elements connected in series.

It can be seen that the R_{gb} is higher than R_b by about an order of magnitude. When pressure increases from 2.6 to 6.6 GPa, the R_b steadily drops with increasing pressure. At the same time, the R_{gb} is also regularly decreasing, and the rate of change is close to linear in this pressure zone. According to these data, it can be seen clearly that the resistance of the bulk is quite different from that of the grain boundary from 2.6 to 6.6 GPa. For example, the resistance at 2.6 GPa is 7.5 MΩ for bulk and 33.2 MΩ for grain boundary, and their difference is as high as 4.4 times. With increasing pressure, for example, at 4.5 GPa, the resistance is 6.9 MΩ for bulk and 15.7 MΩ for grain boundary, a difference of 2.3 times; even at 6.6 GPa, the resistance is 6.7 MΩ for bulk and 12.4 MΩ for grain boundary, and the difference is approximately two times. This difference leads to high density of charges accumulated in the region between the bulk and the grain boundary.[19] Under the circumstances, the dielectric relaxation process can be explained by the Maxwell−Wagner polarization model.[19] When pressure increases to 6.9 GPa, the R_b has an abrupt increase, which reflects the structural phase transition from the tetragonal scheelite phase to the fergusonite phase.[8] As a result of the scheelite-to-fergusonite transition, two Ba−O and W−O bonds are enlarged. R_b of abrupt change is caused by the distortion of the BaO_8 and WO_4 polyhedra.

During the process of alternate current polarization, atoms will deviate from the equilibrium position, and the vibration direction of the electrical dipolar deviates from the phonon coupling direction of lattice vibration, which will then change the dissipation resistance of total lattice vibration. In addition, it is widely acknowledged that the structural effects may strongly influence the observed macroscopic electrical response.[20] The structural phase transition may induce the depletion of the carrier in the grain and make the carrier accumulation at the grain boundary. That is because the defect energy level at the grain boundary can capture the holes and electrons in the grain by the electrical carrier scattering effect of grain boundary.[21] The accumulation of the electrical carrier brings a high-energy barrier and results in the increase of bulk resistance. Meanwhile, the carrier accumulation can bring an increase of carrier concentration at the grain boundary; therefore, more carriers can move through the grain boundary, leading to a decrease of grain boundary resistance.

The decrease of total impedance magnitude indicates that the grain boundary resistance plays a primary role in electrical transport behavior during the phase transition process because of the increase of bulk resistance and decrease of grain boundary resistance. The grain boundary resistance slowly decreases from 6.6 to 7.9 GPa, and no abnormal change occurs. At 7.9 GPa, a fast increase of R_{gb} appears. This abnormal change is also related to the phase transition. As mentioned above, the tetragonal scheelite phase transformed into the monoclinic $BaWO_4$-II phase between 6.9 and 9.5 GPa, and the scheelite-to-fergusonite transition occurred at about 7.5 GPa.[6] The structure of $BaWO_4$-II consists of densely packed networks of distorted WO_6 octahedra. Errandonea et al. interpreted the changes observed at 7.8 GPa as the beginning of a change in the W−O coordination from four to six by X-ray absorption near edge structure detections.[9] The distortion of the W−O

dx.doi.org/10.1021/jp306256k | J. Phys. Chem. C 2012, 116, 25198−25205

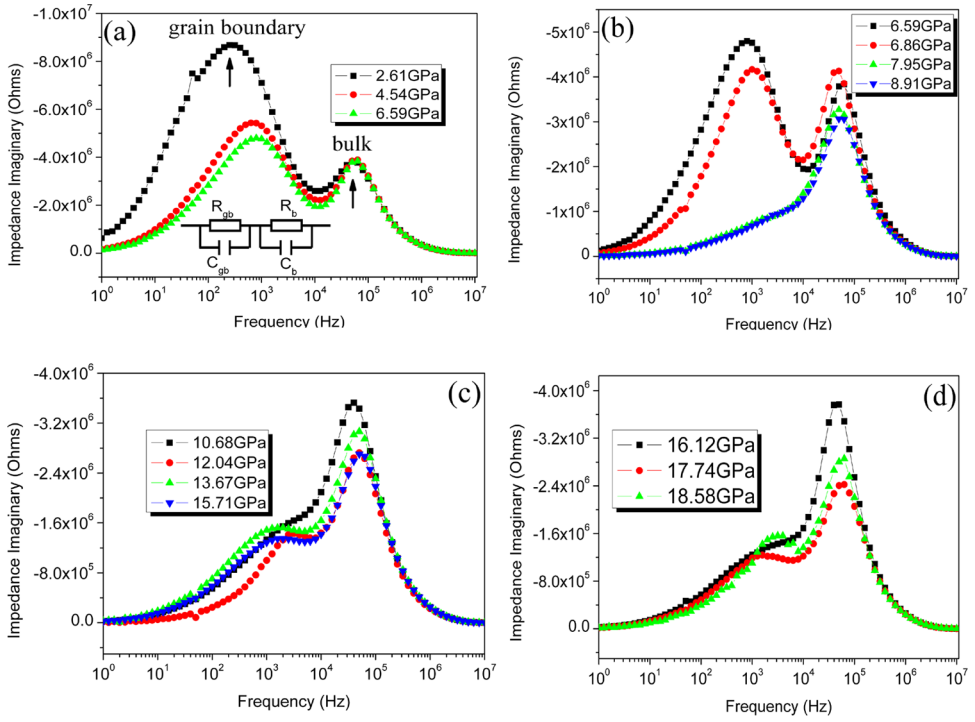

Figure 5. Imaginary parts of the specific impedance Z'' vs frequency under various pressures. Inset: Equivalent circuit models describing intrinsic grain boundary and bulk contributions. The arrows illustrate the grain boundary and bulk relaxation peaks.

tetrahedra is subtle during the transition from scheelite to fergusonite. In fact, the transition is caused by displacements of the Ba cations from their high-symmetry positions in $BaWO_4$ scheelite compounds.[9] With increasing pressure, the R_b has a slowly decreasing trend from 7.9 to 12.6 GPa. There is a minimal bulk resistance when pressure comes up to 12.6 GPa. At the same time, the grain boundary resistance also has a minimal value. The minimal impedance magnitude means that the electrical carrier concentration increases and carrier scattering decreases with increasing pressure. The carrier concentration increases lead to the increase of conductivity, and the lower carrier scattering effect also brings about the increasing conductivity. When pressure comes up to 13.7 GPa, a maximum of bulk resistance is observed. This pressure is related to the phase transition from the fergusonite phase to an unknown phase. Vinod Panchal et al. reported that the compound $BaWO_4$ experienced a phase transition from the fergusonite phase to a disordered structure beyond 14 GPa.[8] The longer and softer Ba−O bonds are more compressible than the shorter and stronger W−O tetrahedral bonds. The heterogeneous compressibility may lead to the different transport rate of the charge carrier.

For $BaWO_4$, two semicircles merge together. The wire inductance has no effect on the impedance, and the correction is not necessary for the sample with lower conductance. Not all impedance curves can show the well-defined semicircle, and some impedance spectra also show an incomplete semicircle in the high-frequency region and a compressed semicircle in the low-frequency region. However, the well-defined semicircles at high and low frequencies are shown in our experiment. The bulk and grain boundary resistances can be fitted by a semicircle, and the intercepts represent the resistances. The change of bulk resistance is different from the variation of grain boundary resistance. In fact, most anomalies of electrical parameters are caused by a pressure-induced phase transition.[10,22] The inflections of bulk and grain boundary resistances indicate the changes of electrical transport properties, which can reflect the structural phase transition under high pressure.

3.2. Pressure-Dependent Relaxation Frequency. The relaxation frequency (f_{max}) is an intrinsic character of the $BaWO_4$ which is independent of its geometrical parameter and susceptible to the grain and grain boundary defects. Figure 5 shows the imaginary part of the impedance as a function of frequency under various pressures. It can be seen that the grain boundary and bulk relaxation peaks are displayed separately at different frequency zones. The relaxation frequency corresponds to the imaginary impedance peak and equals the reciprocal of the time constant. The pattern of variation shows the appearance of peaks at a characteristic frequency dependent on pressure and can be related to the type and strength of the electrical relaxation phenomenon occurring in the sample.

A significant narrowing of the peaks with increasing pressure suggests that the pressure-dependent relaxation process exists in $BaWO_4$. The peak appears to be shifted toward the higher-frequency side with a rise in pressure. The asymmetric narrowing of the peaks may be attributed to the presence of electrical processes in $BaWO_4$ with a spread of relaxation time. From 2.6 to 6.6 GPa, the grain boundary and bulk relaxation frequency gradually increase with increasing pressure, and the relaxation peaks shift to the right [Figure 5(a)]. However, the relaxation peak of the grain boundary is not obviously observed and becomes more and more weak beyond 6.9 GPa in Figure 5(b). The weakening of the relaxation peak indicates that the relaxation process of the grain boundary is impeded. We have also noticed that there is only a single relaxation peak at 7.9 and 8.9 GPa. The frequency region below the peak maximum determines the range in which charge carriers are mobile at long distances. At frequencies above the peak maximum, the carriers are confined to potential wells, being mobile on short

dx.doi.org/10.1021/jp306256k | J. Phys. Chem. C 2012, 116, 25198−25205

Table 2. Fitting Parameters and Calculated Relaxation Frequency under Different Pressures[a]

pressure (GPa)	R_b (ohm)	C_b (F)	R_{gb} (ohm)	C_{gb} (F)	f_b (Hz)	f_{gb} (Hz)
2.61	7.54×10^6	4.07×10^{-13}	3.32×10^7	1.71×10^{-11}	5.19×10^4	2.82×10^2
4.54	6.89×10^6	3.92×10^{-13}	1.57×10^7	1.29×10^{-11}	5.89×10^4	6.78×10^2
6.59	6.65×10^6	3.99×10^{-13}	1.24×10^7	1.31×10^{-11}	6.00×10^4	7.74×10^2
6.86	7.18×10^6	4.77×10^{-13}	1.24×10^7	1.21×10^{-11}	4.65×10^4	1.06×10^3
7.95	6.11×10^6	5.24×10^{-13}	3.92×10^6	6.38×10^{-12}	4.97×10^4	6.37×10^3
8.91	5.66×10^6	5.08×10^{-13}	1.23×10^7	7.96×10^{-13}	5.54×10^4	1.62×10^4
10.68	6.96×10^6	5.86×10^{-13}	8.05×10^6	1.50×10^{-12}	3.90×10^4	1.25×10^4
12.04	5.06×10^6	6.30×10^{-13}	4.71×10^6	2.99×10^{-12}	5.00×10^4	1.13×10^4
13.67	6.07×10^6	5.64×10^{-13}	5.99×10^6	1.20×10^{-11}	4.65×10^4	2.21×10^3
15.71	5.36×10^6	5.76×10^{-13}	5.44×10^6	1.18×10^{-11}	4.94×10^4	2.48×10^3
17.74	5.38×10^6	5.60×10^{-13}	5.62×10^6	1.13×10^{-11}	5.29×10^4	2.50×10^3
18.55	4.77×10^6	5.92×10^{-13}	4.60×10^6	1.38×10^{-11}	5.64×10^4	2.52×10^3

[a]Equation 1 allows determining the relaxation frequency f_{max} (f_b and f_{gb}) from the R and C values for the two RC elements representing the bulk (R_b and C_b) and grain boundary (R_{gb} and C_{gb}) relaxations.

distances.[23] Previous work by Manjón et al. indicated that the $BaWO_4$ microcrystal had a phase transition from the tetragonal scheelite phase to the monoclinic $BaWO_4$-II at about 6.9 GPa[6] so that the discontinuous change in f_{max} is from the phase transition. The rearrangement of atom position leads to the change of polarization mode, and the polarization mode can affect the oscillation frequency, resulting in the change of relaxation frequency. The relaxation peaks of the grain boundary have not been seen from 6.9 to 8.9 GPa in Figure 5(b), but the weak relaxation peak can also be found after 8.9 GPa in Figure 5(c). This is related with the concomitant three phases because the scheelite, $BaWO_4$-II and fergusonite phases coexist from 7.5 to 9.0 GPa. It can be clearly seen that the relaxation peaks have a whole trend of right shift in Figure 5, and the right shift means that the relaxation frequency increases with increasing pressure. There is an obvious left shift for bulk relaxation peaks when pressure comes up to 6.9 GPa. The left shift represents that the relaxation frequency of the bulk has a sudden decrease. Another left shift of the bulk relaxation peak is observed at 13.7 GPa. The two abnormal changes indicate the relaxation process needs more time, and the phenomenon may be related to the recomposition of lattice structure caused by structural phase transitions at about 7 and 14 GPa.

A physically meaningful equivalent circuit could be found to fit the data satisfactorily, and the equivalent circuit model is shown in Figure 5(a). We extracted the measured bulk resistance, capacitance (C_b), grain boundary resistance, and capacitance (C_{gb}) from fitting experimental data by the ZIEW2 impedance analysis software. The relaxation frequency (f_{max}) of the sample as a function of the pressure could be obtained by ac measurements according to the equation[24]

$$f_{max} = \frac{1}{2\pi RC} \quad (1)$$

where R is the resistance and C is the capacitance. Table 2 shows that the bulk relaxation frequency, grain boundary relaxation frequency, and some related parameters under different pressures.

In terms of the data in Figure 6, the bulk relaxation frequency (f_b) gradually increases with increasing pressure from 2.6 to 6.6 GPa. There is a sudden decrease for f_b when pressure comes up to 6.9 GPa. Pressure will bring about the additional energy barrier during the phase transition, which has an effect on the movement of the electrical carrier. The electrical carrier is more difficult to cross the bulk, resulting in the longer time constant.

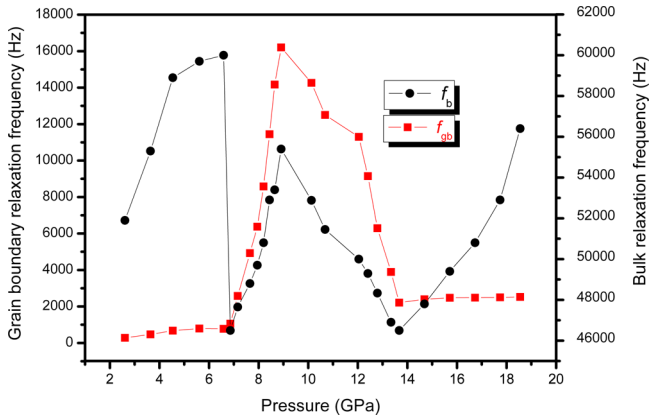

Figure 6. Bulk relaxation frequency (f_b) and grain boundary relaxation frequency (f_{gb}) under various pressures.

The time constant is the reciprocal of relaxation frequency. Therefore, the sudden decrease of bulk relaxation frequency can be directly related to a broad distribution of the relaxation time in the grain inside, and in the meantime it implies a broad distribution of the resistivity.

The increase of defect varieties and the change of lattice structure may also lead to the abrupt decrease of relaxation frequency during the phase transitions. The number of Frenkel and Schottky defects increases because the atoms can be thermally activated caused by the fluctuations of entropy during the phase transition. The f_b has an increasing trend from 6.9 to 8.9 GPa, which is in accordance with previous relaxation peak shifts and caused by the different relaxation time belonging to different kinds of bulk inside. The scheelite, fergusonite, and $BaWO_4$-II phases coexist in this pressure range, in which the fergusonite and $BaWO_4$-II phases have lower relaxation time than the scheelite phase. During the phase transition, the compressure decreases the energy barrier height so that the electrical charge moves more easily in fergusonite and $BaWO_4$-II phases, resulting in the decreasing relaxation time. The average relaxation time leads to an increase of relaxation frequency, and the increasing relaxation frequency also indicates the frequency response property is inductive with increasing pressure.[25]

From 8.9 to 13.7 GPa, the f_b has an obvious decreasing trend, and the condition may be caused by the single phase after the phase transition. The decreasing relaxation frequency also

dx.doi.org/10.1021/jp306256k | J. Phys. Chem. C 2012, 116, 25198−25205

indicates the frequency response property is capacitive with increasing pressure.[26] The f_b also shows the ascending change trend above 13.7 GPa, which means electrical charge resumes to an equilibrium state more quickly after polarization oscillation. Otherwise, the change trend of the grain boundary relaxation frequency (f_{gb}) can be clearly observed in Figure 6. The f_{gb} has an evidently increasing trend from 2.6 to 8.9 GPa. However, the increasing trend is different from the change trend of f_b. The f_{gb} has an inflection above 6.9 GPa, and the rate of the increase for the pressure zone of 6.9−8.9 GPa is steeply higher than the pressure zone of 2.6−6.9 GPa. It can be seen that the f_{gb} starts to decrease with increasing pressure beyond 8.9 GPa. This trend may be related to the end of the scheelite-to-fergusonite transition at about 9.0 GPa. This result indicates the f_{gb} is also sensitive to the phase transition process compared with the f_b because of a similar change trend but larger relaxation frequency. The f_{gb} has a decreasing trend after 8.9 GPa. This indicates that the grain boundary relaxation process becomes longer than before the phase transition.

When an electric current passes through interfaces between the bulk and grain boundary due to their different conductivities, grain surface charges pile up at the interfaces and give rise to a Debye-like relaxation process under an external alternating voltage.[27] However, a discontinuous f_{gb} occurs and starts to increase when pressure comes up to 13.7 GPa. This can be explained with the dipole relaxation model associated with the crystal structure.[28] It is presumed that the structural phase transition leads to the electrical charge rearrangement on the grain boundary, and a core with two adjacent space charge layers has been formed.[29,30] The electrical charge rearrangement resumes to the equilibrium state more quickly and needs the shorter relaxation time, resulting in the stabilization of the space charge layer at the grain boundary surface. From 13.7 to 18.6 GPa, the f_{gb} keeps smoothly increasing with increasing pressure. The regular variation of ac conductivity indicated that the conduction occurs by hopping of charge carriers and small polarons among localized states.

3.3. Pressure-Induced Activation Energy. The relaxation frequencies of the bulk and grain boundary can be expressed according to the Arrhenius law

$$f = f_0 \exp(-E/k_B T) \quad (2)$$

where E represents the activation energy; k_B is the Boltzmann constant; and T is the temperature. If the temperature remains at room temperature, f and E are only functions of pressure, and f_0 is the prerelaxation factor and remains constant, the following equation can be obtained

$$d(\ln f/dP) = \partial(\ln f_0)/\partial P - (1/k_B T)(\partial E/\partial P) \quad (3)$$

By linear fitting to the curve ln f~P, we obtained the pressure dependence of the activation energy shown in Figure 7. Actually, the relaxation frequency represents the charge−discharge rate of the dipole oscillation process, and its activation energy denotes the energy to activate the resonance. The activation energy of bulk indicates that the vibration damping of W−O dipoles is weakened in the pressure zone of 6.9−8.9 GPa and above 13.7 GPa. The relative displacements of neighboring W and O ions against each other at higher pressure make the valence electrons more polarizable and localized. The electron localization affects the hybridization of the W and O orbital and results in a large dipole moment

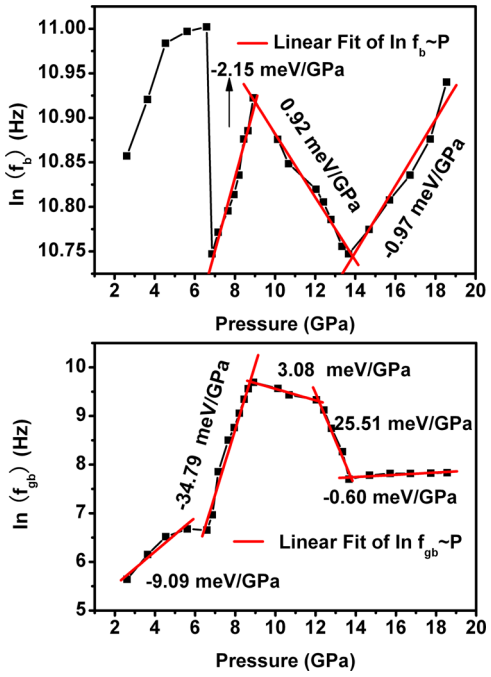

Figure 7. Activation energy of the bulk and grain boundary under different pressure ranges by linear fit of ln f~P.

associated with the W−O bond in the pressure zone of 6.9−8.9 GPa and above 13.7 GPa.

For the grain boundary, the pressure dependence of the activation energy is −9.09 meV/GPa from 2.6 to 6.9 GPa, indicating that the activation energy of the grain boundary decreases with increasing pressure. The activation energy of the grain boundary decreases from 6.9 to 8.9 GPa, and then the rate of decrease is much larger compared with the pressure zone of 2.6−6.9 GPa. This indicates that in the pressure range of 2.6−8.9 GPa the pressure has a negative contribution to the activation energy, and the transport of charge carriers through the boundary becomes easier. Above 8.9 GPa, on the contrary, the activation energy increases with pressure. This indicates that in the pressure range of 8.9−13.7 GPa the pressure has a positive contribution to the activation energy and makes the transport of charge carriers difficult. After structural phase transition beyond 13.7 GPa, the activation energy also decreases with increasing pressure and makes the transport of charge carriers easy.

4. CONCLUSION

In summary, we performed in situ high-pressure electrical transport behavior of Barium tungstate up to 20 GPa by alternate current impedance spectrum techniques. The bulk and grain boundary effects were separated by fitting the equivalent circuit. The grain boundary effect plays a prominent role in the electrical transport process, and the bulk contribution is subordinate. The structural phase transitions lead to the discontinuous changes of bulk and grain boundary resistance at about 7 and 14 GPa. The impedance bulk arcs indicate a structural transition is first caused by bulk and then is involved in the grain boundary at about 7 GPa. The abrupt variations of relaxation frequency for bulk and grain boundary are also caused by the structural phase transitions. The decreasing activation energy of the grain boundary shows that the pressure has a negative contribution to the activation

dx.doi.org/10.1021/jp306256k | J. Phys. Chem. C 2012, 116, 25198−25205

energy, and the transport of charge carriers through the boundary becomes easier from 6.9 to 8.9 GPa. In addition, the ascending relaxation frequency of the bulk and grain boundary indicates that the polarization process needs much shorter time during the phase transitions between 6.9 and 8.9 GPa.

■ ASSOCIATED CONTENT

Supporting Information

Tables showing the parameters of experimental equipment and setup. This information is available free of charge via the Internet at http://pubs.acs.org.

■ AUTHOR INFORMATION

Corresponding Author

*Phone: +86-431-85168878-601. Fax: +86-431-85168878-602. E-mail: cxgao599@yahoo.com.cn.

Notes

The authors declare no competing financial interest.

■ ACKNOWLEDGMENTS

This work was supported by the National Basic Research Program of China (2011CB808204), the National Natural Science Foundation of China (11074094, 91014004, 11164031), and the Special Scientific Research Funding for Doctoral Discipline in Higher Education Institutions (200801831007).

■ REFERENCES

(1) Errandonea, D.; Manjón, F. J.; Garro, N.; Rodríguez-Hernández, P.; Radescu, S.; Mujica, A.; Muñoz, A.; Tu, C. Y. *Phys. Rev. B* **2008**, *78*, 054116 1−16.

(2) Lima, R. C.; Anicete-Santos, M.; Orhan, E.; Maurera, M. M.; Souza, A. G.; Pizani, P. S.; Leite, E. R.; Varela, J. A.; Longo, E. *J. Lumin.* **2007**, *126*, 741−746.

(3) Basiev, T. T.; Sobol, A. A.; Zverev, P. G.; Osiko, V. V.; Powell, R. C. *Appl. Opt.* **1999**, *38*, 594−598.

(4) Černý, P.; Zverev, P. G.; Jelínková, H.; Basiev, T. T. *Opt. Commun.* **2000**, *177*, 397−404.

(5) Lacomba-Perales, R.; Ruiz-Fuertes, J.; Errandonea, D.; Martínez-García, D.; Segura, A. *Europhys. Lett.* **2008**, *83*, 37002 1−5.

(6) Manjón, F. J.; Errandonea, D.; Garro, N.; Pellicer-Porres, J.; Rodríguez-Hernández, P.; Radescu, S.; López-Solano, J.; Mujica, A.; Muñoz, A. *Phys. Rev. B* **2006**, *74*, 144111 1−17.

(7) Jayaraman, A.; Batlogg, B.; VanUitert, L. G. *Phys. Rev. B* **1983**, *28*, 4774−4777.

(8) Panchal, V.; Garg, N.; Chauhan, A.; Sangeeta; Surinder; Sharma, S. M. *Solid State Commun.* **2004**, *130*, 203−208.

(9) Errandonea, D.; Pellicer-Porres, J.; Manjón, F. J.; Segura, A.; Ferrer-Roca, C.; Kumar, R. S.; Tschauner, O.; López-Solano, J.; Rodríguez-Hernández, P.; Radescu, S.; et al. *Phys. Rev. B* **2006**, *73*, 224103 1−15.

(10) Han, Y. H.; Gao, C. X.; Ma, Y. Z.; Liu, H. W.; Pan, Y. W.; Luo, J. F.; Li, M.; He, C. Y.; Huang, X. W.; Zou, G. T.; et al. *Appl. Phys. Lett.* **2005**, *86*, 064104 1−3.

(11) Li, M.; Gao, C. X.; Ma, Y. Z.; Wang, D. J.; Li, Y. C.; Liu, J. *Appl. Phys. Lett.* **2007**, *90*, 1135071−3.

(12) Piermarini, G. J.; Block, S.; Barnett, J. D.; Forman, R. A. *J. Appl. Phys.* **1975**, *46*, 2774−2780.

(13) Nobre, M.; Lanfredi, S. *J. Appl. Phys.* **2003**, *93*, 5576−5582.

(14) Schmidt, R.; Wu, J.; Leighton, C.; Terry, I. *Phys. Rev. B* **2009**, *79*, 125105 1−8.

(15) Li, M.; Yang, J.; Snoussi, K.; Li, L. X.; Wang, H. X.; Gao, C. X. *Appl. Phys. Lett.* **2010**, *97*, 174101 1−3.

(16) Ruffo, R.; Hong, S. S.; Chan, C. K.; Huggins, R. A.; Cui, Y. *J. Phys. Chem. C* **2009**, *113*, 11390−11398.

(17) Lin, Y. H.; Li, M.; Nan, C. W.; Li, J. F.; Wu, J. B.; He, J. L. *Appl. Phys. Lett.* **2006**, *89*, 032907 1−3.

(18) He, L.; Ling, Z. Y. *Appl. Phys. Lett.* **2011**, *98*, 242112 1−3.

(19) Ang, C.; Yu, Z. *Appl. Phys. Lett.* **2007**, *90*, 2029031−3.

(20) Garcia-Belmonte, G.; Bisquert, J.; Pereira, E. C.; Fabregat-Santiago, F. *Appl. Phys. Lett.* **2001**, *78*, 1885−1887.

(21) Li, Y. Q.; Gao, Y.; Han, Y. H.; Wang, Q. L.; Su, N. N.; Zhang, J. K.; Liu, C. L.; Ma, Y. Z.; Gao, C. X. *J. Phys. Chem. C* **2012**, *116*, 5209−5214.

(22) Wang, Q. L.; Han, Y. H.; Liu, C. L.; Ma, Y. Z; Ren, W. B.; Gao, C. X. *Appl. Phys. Lett.* **2012**, *100*, 172905. 1−4.

(23) Dutta, A.; Sinha, T. P.; Shannigrahi, S. *Phys. Rev. B* **2007**, *76*, 155113 1−7.

(24) Srinivas, K.; James, A. R. *J. Appl. Phys.* **1999**, *86*, 3885−3889.

(25) Kazimierczuk, M. K.; Sancineto, G.; Grandi, G.; Reggiani, U.; Massarini, A. *Ieee Trans. Magn.* **1999**, *35*, 4185−4191.

(26) Bülbül, M. M.; Zeyrek, S. *Microelectron. Eng.* **2006**, *83*, 2522−2526.

(27) Zhang, H. T.; Deng, X. Y.; Li, T.; Zhang, W.; Chen, R.; Tian, W. W.; Li, J. B.; Wang, X. H.; Li, L. T. *Appl. Phys. Lett.* **2010**, *97*, 162913 1−3.

(28) Sinclair, D. C.; Adams, T. B.; Morrison, F. D.; West, A. R. *Appl. Phys. Lett.* **2002**, *80*, 2153−2155.

(29) Kjølseth, C.; Fjeld, H.; Prytz, Ø.; Dahl, P. I.; Estournès, C.; Haugsrud, R.; Norby, T. *Solid State Ionics* **2010**, *181*, 268−275.

(30) Kim, S.; Fleig, J.; Maier, J. *Phys. Chem. Chem. Phys.* **2003**, *5*, 2268−2273.